Research Article

Analice Turski Silva Diniz and Bernhard Schartel*

# The effects of property variation on the dripping behaviour of polymers during UL94 test simulated by particle finite element method

https://doi.org/10.1515/epoly-2023-0194
received December 15, 2023; accepted January 30, 2024

**Abstract:** The dripping behaviour of polymers is often observed experimentally through the UL94 flammability standard test. In this work, polymeric dripping under fire is investigated numerically using particle finite element method. A parametric analysis was carried out to observe the influence of a single property on overall dripping behaviour via a UL94 vertical test model. Surrogates and property ranges were defined for variation of the following parameters: glass transition temperature ($T_g$), melting temperature ($T_m$), decomposition temperature ($T_d$), density ($\rho$), specific heat capacity (Cp), apparent effective heat of combustion of the volatiles, char yield ($\mu$), thermal conductivity ($k$), and viscosity ($\eta$). Polyamide, poly(ether ether ketone), poly(methyl methacrylate), and polysulfone were used as benchmarks. Simulated results showed that specific heat capacity, thermal conductivity, and char yield allied with viscosity were the properties that most influenced dripping behaviour (starting time and occurrence).

**Keywords:** dripping, PFEM, UL 94, simulation, fire behaviour

## 1 Introduction

Melt flow and dripping can interfere with the classification of polymers in flammability testing (1). This is true for the UL 94 vertical test (2), where the ability of a small plastic part to extinguish or spread the flame after ignition is measured. There the specimen is exposed to a small flame, and the measured burning time, whether the fire reaches the clamp, and the presented dripping are the standard criteria for a material's classification. If a material passes the first two criteria, the dripping condition (as flaming drops, non-flaming drops, or no dripping) delivers three different ratings: V-2, V-1, or V-0. The most desirable rating in flame retardancy is V-0, basically meaning extinction within 10 s with no dripping or with non-flaming drips. The classifications V-1 and V-2 allow extinction within 30 s and non-flaming and flaming drips, respectively. For this reason, the UL 94 test has been proposed for a quantitative and qualitative investigation of dripping behaviour (3). Based on safety requirements, the UL 94 classifies the usability of the materials for specific end-uses, such as in electrical equipment and products.

Melt flow and dripping are a physical response to the chemical process of polymeric combustion. Heat and fuel are removed from the pyrolysis zone. Thus, dripping competes with gasification and charring (4). Many factors can lead or contribute to favouring dripping over the other mentioned responses, namely, the sample dimensions, the polymeric properties (chemical and physical), the material composition (influence of blending and additives, such as fillers, nanomaterials, and flame retardants), and the mechanism of decomposition involved (type of chain scission, released volatiles/products, cross-linking, and residue formation) (3–26). Experimental observation of the dripping phenomenon is fundamental for understanding its specific causes in each polymeric system.

A common agreement among different works on several polymers that investigate dripping is that viscosity at low shear rates may be the main factor governing dripping behaviour (20–23). This is suggested by the observation that adjustments to the viscosity of a melting or decomposing material can lead to a flow limit (4,5,8,11). This is of great interest where the main goal is to develop new ways to minimize dripping and to improve UL94 test classification of polymeric products as well (6–10), especially to prevent dripping in V-0 classified materials (20) and to enhance non-flaming dripping in V-0 classified materials too (27,28). To achieve these objectives, more knowledge of

* **Corresponding author: Bernhard Schartel**, Bundesanstalt für Materialforschung und -prüfung (BAM), Unter den Eichen 87, 12205 Berlin, Germany, e-mail: bernhard.schartel@bam.de
**Analice Turski Silva Diniz:** Bundesanstalt für Materialforschung und -prüfung (BAM), Unter den Eichen 87, 12205 Berlin, Germany

viscosity's role in dripping is necessary. In the experimental approach, for example, the quest is for suitable polymeric systems: finding the adequate additive, in the right amount, that will perform in the desired way (accounting for chemical interactions) to exert the expected restriction on dripping, while maintaining the properties required for its application (18,20,21,29–31). This path applies to investigating any other potentially relevant property so that its behaviour can be understood through experimentation. New methods of measurement may be developed as well. The process is costly, but it is necessary to acquire information about new developments. Nevertheless, numerical tools can help this knowledge expand faster through the use of a reversed approach: from properties (or cause) to dripping.

Particle finite element method (PFEM) is a numerical tool developed to solve complex fluid-structure problems (32). As described, the burning process can be an intricate problem because of the various interactions in intermediate stages. A solid polymer may be converted into different states of matter during burning, due to processes including heat transfer and material decomposition. Accordingly, when the polymeric material part is in a suspended position, there is the possibility of fluid flow. PFEM can treat the polymer as a structure and as a fluid, covering the problem of fluid drops separating from a solid portion of the material (33). This computational method has been used to successfully predict the dripping behaviour of polymeric materials under testing conditions, such as in the EN 50399 bench-scale test for cables (34) and in the UL94 vertical standard test (4,22,27,35,36). However, the influence of viscosity has been reported as a factor limiting improved predictions (36).

In this work, a parameter analysis was performed using PFEM. The impact of input parameters (polymer properties) on dripping behaviour (starting time and number of occurrences during the full simulated time) was investigated. Precisely, the effect of different viscosities, transition temperatures (glass, melting, and decomposition temperatures), char yields, densities, thermal conductivities, apparent effective heats of combustion, and Arrhenius parameters (activation energy and pre-exponential factor) on dripping was observed. The simulated findings were compared to some experimental data (benchmarks) and literature data.

# 2 Experimental

## 2.1 Numerical approach

The PFEM (32) was the computational method chosen to execute this parameter analysis work on dripping behaviour. In contrast to the Fire Dynamic Simulator and ThermaKin tools – which had parametric studies on mass loss rate (37–39) and recently a developed model for UL94 test (40,41), the PFEM uses an updated Lagrangian description to address complex problems between fluid and solid mechanics, such as large deformations, coupled thermal effects, immiscible interactions, fragmentation, melting, and dripping, among others (42). The method combines standard finite element method with particle-based techniques. In the PFEM, the analysed mesh domain is formed by discretized boundaries and nodes. The nodes carry all of the material information (properties) as small material particles (points). These points can move freely and can even separate from the main domain of analysis. Under the modelled condition, nodes are tracked during the transient solution. Then the boundaries are redefined accordingly by the Alpha-Shape algorithm (35,33), and the mesh is regenerated at the new position. State variables are solved, and the motion equations are solved again, such that the domain is updated at each time step. Details on the governing equations and the discrete equations, as well as PFEM general code details, are given elsewhere (35,42).

The modelled scenario was based on the UL94 vertical test. A 3D specimen geometry with the dimensions of 125.0 × 6.5 × 1.5 $mm^3$ was generated with GiD software (version 15.1.6.d). It contained 3,285 nodes and 12,095 tetrahedral elements. The velocities were fixed on the top of the specimen to model clamping. The simulation consisted of 10 s of flame application plus 20 s of after-flame time. It corresponded to an observation of both the first ignition and the first after-flame time of the UL94 vertical test. The starting temperature of the specimen is set to 298 K. The heat flux Q1 due to the flame of the burner and the heat flux Q2 from flame due to burning polymer are applied to the specimen bottom tip. The maximum heat intake by the flame was set to 150 $kW \cdot m^{-2}$ (43). It was applied as an exponentially decreased function at the bottom of the specimen. The total heat intake of the specimen due to the burner was set to ~ 48 W. In addition, heat flux due to combustion of the pyrolysis gases was determined. Gasification was based on the product of density, heat of decomposition, and volume variation. Heat feedback corresponded to the heat release rate (HRR) calculation of the material (the product of the mass loss rate and apparent effective heat of combustion). The apparent effective heat of combustion was the product of the heat of combustion of the volatiles and the combustion efficiency. The HRR was reduced by the char yield. Charring is considered as storage of fuel competing with fuel release and heat production. The thermal decomposition kinetics is described by a one-step, first-order Arrhenius equation. During the after-flame time (the following 20 s)

only Q2 is applied, taking into account the removal of the burner. The maximum heat flux at the bottom by the flame remains set to 150 $kW \cdot m^{-2}$. More details on the boundary conditions of the model can be found in ref. (4).

The input parameters for PFEM simulation are the following: viscosity, activation energy and Arrhenius coefficient of decomposition, char yield, density, effective heat of combustion, heat of decomposition, specific heat capacity, and thermal conductivity of the material. The simulation materials (surrogates) were designed considering all these parameters. These polymers comply with the dependency relation between viscosity and key temperatures. To identify the influence of each parameter on dripping behaviour, they were varied under a selected range specified below in Section 2.3. The combustion efficiency was set to 1 for all surrogates developed, neglecting fuel dilution and flame inhibition effects. The results for the dripping time were set to seconds relinquishing digits after the point to make the identification of the property effects easy and reliable during the simulation time (30 s). By the way, dripping times in seconds enable also the reasonable comparison with other experimental and simulating works analysing dripping (12,16,22).

## 2.2 Benchmarks

Four thermoplastics were experimentally evaluated for this work: polysulfone – PSU (Ultrason® S2010, BASF), poly(ether ether ketone) – PEEK (450 G, Victrex™), polyamide 6 – PA6 (Technyl® S27 BL, Solvay), and poly(methyl methacrylate) – PMMA (Pexiglas®). The UL-94 vertical test was performed according to (2) using specimens with the dimensions of 125.0 × 13.0 × 3.0 $mm^3$. The small-scale test was recorded by a conventional digital camera to ease dripping quantification. An infrared camera was also used to monitor heat spread (Therma CAM S65 FLR).

Most of the other material properties were obtained through measurements. Density was obtained from a sample's weight and dimensions. Thermal transitions were observed via differential scanning calorimetry (DSC) performed using a NETZSCH DSC 204F1 Phoenix at a heating rate of 10°C·$min^{-1}$ from −50°C to 35°C under a nitrogen atmosphere (50 mL·$min^{-1}$), using samples in pellet form (8.0 ± 0.1 mg). The decomposition was assessed via thermogravimetric analysis (TGA) performed using a NETZSCH TG 209F1 under 30 mL·$min^{-1}$ nitrogen flow, heating from 2°C to 90°C at a heating rate of 10°C·$min^{-1}$ using samples in powder form (10.0 ± 0.1 mg). Thermal conductivity was measured according to ISO 22 007 in a TPS 1500 Hot Disk instrument using the transient plane heat source method. A sensor with a radius of 3.189 mm was used on fire test specimens. The specific heat capacity was determined via DSC in accordance with the ISO 11357-4 standard. The heat of decomposition was taken from the literature (44). The effective heat of combustion of the volatiles was determined via a cone calorimeter (FTT equipment) under a heat flux of 50 $kW \cdot m^{-2}$. Parameters of the decomposition kinetics were obtained from TG data of the materials measured at different heating rates (2, 5, 10, and 20°C·$min^{-1}$), according to ASTME698. Rheological properties were measured in a plate-plate rheometer (MCR 501, Anton Paar) in oscillation mode, with an angular frequency of 100–0.1 rad·$s^{-1}$ and a deformation amplitude of 0.5%, using samples in pellet form. The temperature of rheological measurements differed for each material and was set to one above the melting temperature and under the decomposition temperature.

## 2.3 Viscosity setup

Viscosity is the most important parameter controlling dripping. The rheological response of the materials to heat is a critical input to the dripping problem in the PFEM tool. From the temperature calculated for each node, the viscosity as a function of temperature can be continuously updated in the domain.

To study both the impact of viscosity and the impact of other properties on dripping, viscosity must be estimated as a function of temperature. Therefore, base curves for the surrogates were proposed (Figure 1). They were based on rheology data from our selected benchmarks (PA6, PEEK, PSU, and PMMA) and on published data for polypropylene (PP) (14,35), polycarbonate/acrylonitrile–butadiene–styrene (4), polyamide 4.6 (PA46) (22), and intumescent coatings (45). These base curves consist of two types of viscosity reduction (curves 1 and 2), and the same two types of main reduction followed by a rise (curves 1.c and 2.c). *Curve 1* represents a steeper decline, while *curve 2* represents a more gradual decline. Among the evaluated thermoplastic materials, there was a tendency for amorphous materials to perform like *curve 1*, and for semi-crystalline materials to perform the way approximated by *curve 2*. The rise in the viscosity of *curve 1.c* and *curve 2.c* is attributed to cross-linking and char formation in amorphous and semi-crystalline materials, respectively. In a comprehensive way, these four curves correspond with the flow behaviour of most thermoplastics.

The flow curves begin from the solid state, which was set to $10^7$ Pa·s for all materials. In different curves, the glass transition temperature ($T_g$) and the melting temperature

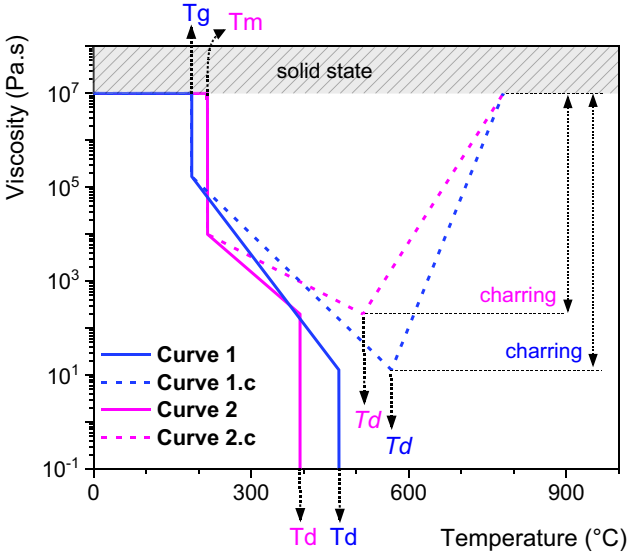


**Figure 1:** Proposed flow curves for different thermoplastic materials (simulation surrogates).

($T_m$) were set as the first point of transition from the solid to the fluid state of the thermoplastics. These are the first points where the decreased resistance to flow can favour dripping/melt flow. For amorphous thermoplastics (curves 1 and 1.c), the starting point of the decrease in viscosity is clearly the glass transition temperature ($T_g$). Despite the existence of a $T_g$ in semi-crystalline materials as well, it makes the material bonds more flexible but does not necessarily allow flow. This is the case for materials such as PEHD, PELD, and PP, for example, which have $T_g$ values below °C, and are softer at room temperature but remain in the solid state. Matzen et al. showed that dripping below $T_m$ resulted from regions of the specimen that became soft (20). Moreover, our recent study showed that the $T_m$ has much greater impact than $T_g$ on the dripping behaviour under fire of polyamide 4.6 – a semi-crystalline material (22). Accordingly, the starting point of the significant decrease in viscosity for semi-crystalline thermoplastics adopted here was the melting temperature ($T_m$).

The second transition point set was the decomposition temperature ($T_d$). In several rheological measurements, a small viscosity plateau of low value was observed between the onset and end of $T_d$. Here, this plateau was neglected and only one point of transition was used. This was the point of most conversion, the temperature of the peak of decomposition obtained from dTG curves (from TGA). Viscosity increases after $T_d$ for charring polymers, while viscosity reaches zero after $T_d$ for non-charring polymers. Most drops generated under fire form after the decomposition temperature is reached, due to the extremely high heating rate of the fire. Evaluation revealed that the drops contain melted and decomposed polymer. In flaming drops, the presence of decomposed material is increased (21).

In Figure 1, the temperature resistances differ between the respective pairs of materials (*curve 1/1c* and *curve 2/2c*). Charring polymers tend to be more resistant than non-charring polymers, as can be seen in the temperatures in Table S1. Table S1 shows the selected ranges of transition temperatures to be simulated in this work based on Lyons's data for several polymers (46). The viscosity function at PFEM is applied according to the polymeric temperature reached during test.

The other input parameters necessary for simulation are displayed in Table 1. The surrogate was defined based on a range of values found for thermoplastics (38,39,46). The Arrhenius coefficient ($A$) and activation energy ($E_a$) were set according to the $T_d$ utilized and not subjected to further independent variation, due to their correlation (38). In Table 2, charring and non-charring versions of the surrogate (Table 1) were defined according to their viscosity and temperatures. No additional structural differentiation was made between charring and non-charring materials in the model. Parameters were considered being rather independent from each other; this fundamental approach was chosen to vary properties in their reasonable range but independently from each other. Links such as aromatic structures in the main chain yield higher softening temperatures and higher char yields are not used. The exact flow curves depicted in Figure 1 are those from the designed surrogates of Table 2. Simulations were named as *am* – amorphous, *am_c* – amorphous charring, *sc* – semi-crystalline, and *sc_c* – semi-crystalline charring. The impact of charring on the viscosity is taken into account as the most important phenomenon but without establishing it as function of the char yield.

**Table 1:** Range of polymeric input parameters and the selected values for surrogates

| Input parameter | Range | Surrogate | Units |
|---|---|---|---|
| Density ($\rho$) | 800–2,200 | 1,100 | $kg{\cdot}m^{-3}$ |
| Thermal conductivity ($k$) | 0.10–0.45 | 0.27 | $W{\cdot}m^{-1}{\cdot}K^{-1}$ |
| Specific heat capacity (Cp) | 900–2,100 | 1,500 | $J{\cdot}kg^{-1}{\cdot}K^{-1}$ |
| Activation energy ($E_a$) | 100–300 | 200 | $kJ{\cdot}mol^{-1}$ |
| Arrhenius coefficient ($A$) | $2.0 \times 10^9$–$5.0 \times 10^{21}$ | (see Table 2) | $s^{-1}$ |
| Char | 0–68 | (see Table 2) | % |
| Effective heat of combustion (EHC) | 4–45 | 25 | $MJ{\cdot}kg^{-1}$ |
| Heat of decomposition ($H_{dec}$) | 800–2,600 | 1,700 | $kg{\cdot}J{\cdot}kg^{-1}$ |

**Table 2:** Types of surrogates designed for simulations

| Simulation* | Viscosity** | $T_g$ (°C) | $T_m$ (°C) | $T_d$ (°C) | A ($s^{-1}$) | Char yield |
|---|---|---|---|---|---|---|
| *Am* | 1 | 187 | | 467 | $1.30 \times 10^{12}$ | — |
| *am_c* | 1.c | 187 | | 567 | $2.70 \times 10^{10}$ | 30 |
| *Sc* | 2 | — | 217 | 393 | $4.80 \times 10^{13}$ | — |
| *sc_c* | 2.c | — | 217 | 513 | $1.90 \times 10^{11}$ | 30 |

*Nomenclature: *am* – amorphous, *am_c* – amorphous charring, *sc* – semi-crystalline, *sc_c* – semi-crystalline charring.
**Curve denominations from Figure 1.

# 3 Results and discussion

Results of simulation runs are illustrated by graphs of time vs dripping occurrence. These indicate the occurrence of dripping in a specific time (in seconds) during the simulation, but the number of drops generated in each of those occurrences was not discretized in the work. This choice was made to focus on dripping resistance rather than quantification. The work addresses drip prevention as the greatest goal by identifying the most important factors (properties) triggering the occurrence of dripping.

## 3.1 Surrogates

As shown in Figure 2a, a nearly steady production of drops is observed. This non-stop dripping behaviour is attributed to the response of the surrogates' overall properties (especially the parameters of decomposition kinetics) to the heat fluxes applied. From the evaluation of temperatures reached by the tip of the specimens (calculated for each node of the generated mesh – shown in Figure 2b – at each time step), burning behaviour was identified after removal of the Bunsen flame.

The *am* simulation started to drip during application of the flame (at 7.0 s), while the *sc* simulation started dripping after the first 10 s (at 13.0 s). This indicates a better resistance to flow for simulated *sc*. Over the same total testing time (30 s), the production of drops was slightly higher for *sc* than for *am*. When the two simulated specimens' tips were compared at the same simulation time (Figure 2c and d), it became clear that *am* lost more mass due to dripping and gasification than *sc*. In this example, at 20 s, the *am* specimen tip presented a maximum temperature of 366°C (Figure 2c), which is below $T_d$ (46°C), while *sc* had a maximum temperature of 432°C (Figure 2d), which is above $T_d$ (393°C). At this point, the drops generated by *am* could be considered melt dripping, while the dripping generated by *sc* was a product of decomposition. However, the low temperature of *am* in this specific simulation time was related to a release of heat from the previous dripping (at 19 s). Thus, the complexity of dripping quantification and evaluation is also depicted numerically.

A stair-step characteristic emerged in the curves when a higher interval of time between two dripping occurrences was observed. This was attributed to a previous large mass loss due to dripping which liberated heat and then to the new heat accumulation time until the next drip. The repeated process of mass and heat accumulation through the advancement of the melting front and the total heat flux leading to dripping was reported by ref. (47).

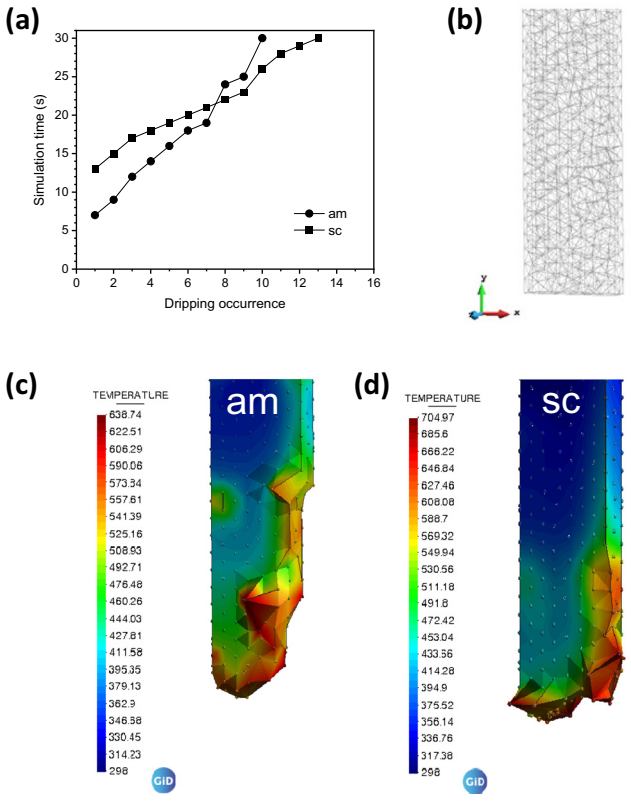


**Figure 2:** (a) Results of the *am* and *sc* simulation; (b) specimen tip of the initial ($t$ = 0 s) mesh model; (c) the *am* specimen tip at $t$ = 20 s with achieved temperatures (in Kelvin), and (d) the *sc* specimen tip at $t$ = 20 s with achieved temperatures (in Kelvin).

The viscosity curve and the transition temperatures used in the surrogates influenced the dripping starting time and the dripping occurrence. Further investigations on $T_g$, $T_m$, and $T_d$ variation were performed to better understand this influence.

## 3.2 Transition temperatures

Figure 3 shows the collection of results from varying transition temperatures. All temperatures applied were chosen from the range reported in Table S1. When the first transition temperature ($T_g$ or $T_m$) was varied, the decomposition temperature remained the same, and *vice-versa*.

Four *am* simulations were performed at varying glass transition temperatures ($T_g$) (Figure 3a). Increasing the $T_g$ slightly increased the delay to the start of dripping (from 3 to 7 s). This minor difference was attributed to the sharp decline in viscosity applied for *am* simulation, which allowed the dripping flow to start easily/quickly after any $T_g$ value was achieved. A reduction in the occurrence of dripping was also observed when $T_g$ was increased from 10°C to 18°C (from 21 to 10 occurrences). This corresponds with the idea that the higher the transition temperature, the higher the dripping resistance. However, for the highest $T_g$ value (22°C) dripping increased again to 13 occurrences, a probable effect of the increased proximity to the decomposition temperature ($T_d$).

Five *sc* simulations were run with different melting temperatures ($T_m$). The results are shown in Figure 3b. $T_m$ values of 10°C and 16°C had dripping start at 8 and 6 s, respectively. After that, an increase in the $T_m$ value resulted in an increased delay in the time at which dripping started. The differences between dripping starting

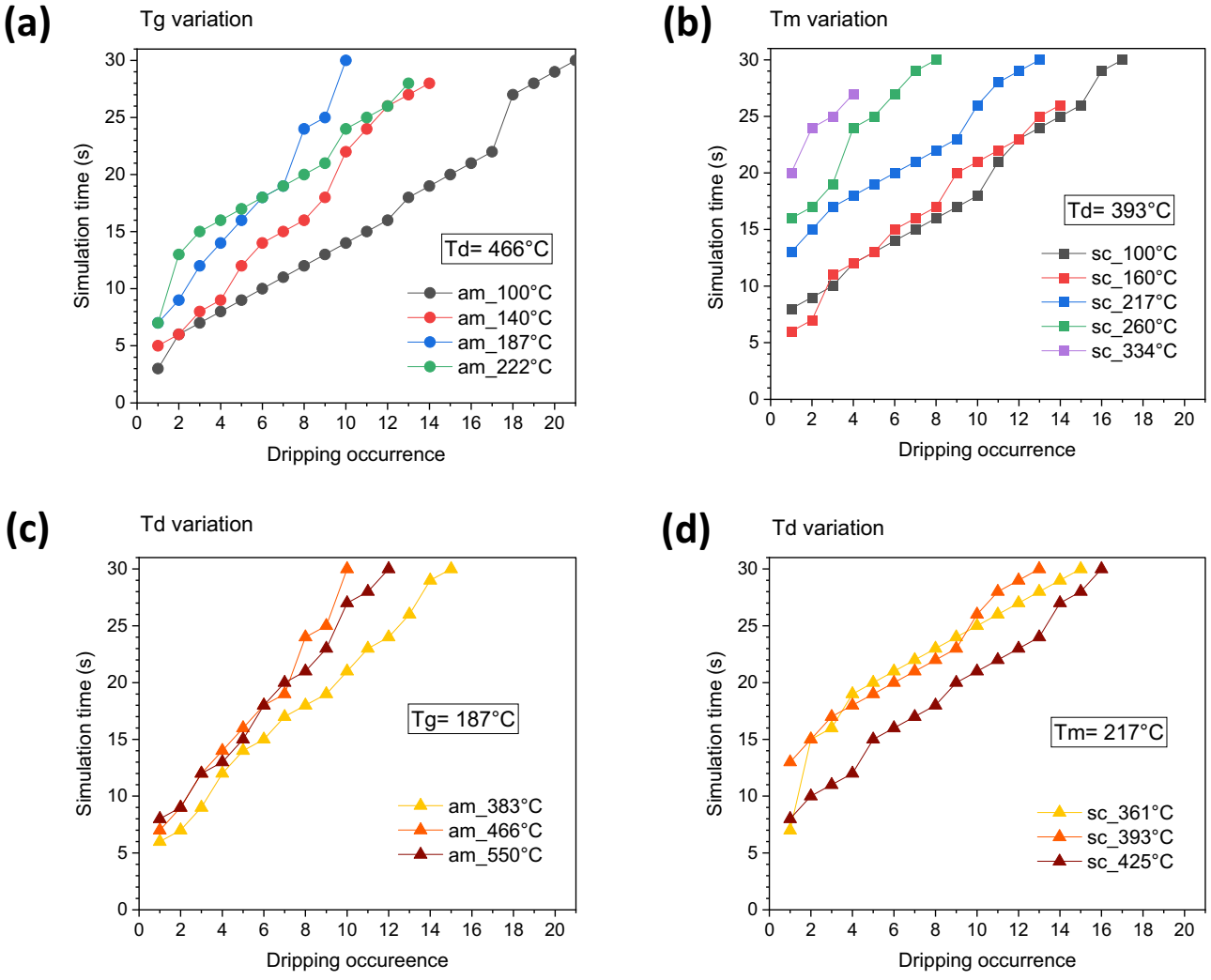


**Figure 3:** Results of varying the transition temperatures, (a) $T_g$, (b) $T_m$, (c) $T_d$ for $T_g$ = 187°C, and (d) $T_d$ for $T_m$ = 217°C.

times were very significant in this case; for $T_m$ 33°C, the dripping started only at 20 s. With the exception of $T_m$ 16°C, the higher the $T_m$, the lower the occurrence of dripping (from 17 to 4). Thus, in *sc* simulations, the dripping occurrence at the highest $T_m$ value (33°C) was not affected by its proximity to $T_d$ (39°C). The reason seems to be that after the specimen reached $T_m$, the gradual decline in the viscosity applied to *sc* offered more resistance to droplet flow up to $T_d$ than in the *am* materials.

To assess $T_d$ variation, the non-charring surrogates (*am* and *sc*) were used. For *am* simulations (Figure 3c), no major alteration in the start of dripping was observed for the three different $T_d$ applied: the dripping start shifted to 6, 7, and 8 s when $T_d$ was increased. The decreasing order of dripping occurrence observed was as follows: the lowest $T_d$ value produced the most dripping occurrences (15), followed by the highest $T_d$ (12), and the middle value of $T_d$ (10). For *sc* simulations (Figure 3d), the highest and the lowest $T_d$ values had a similar delay in dripping start (7 and 8 s, respectively), as compared to the middle value of $T_d$ (13 s). As for *am*, the middle value of $T_d$ applied to *sc* had fewer dripping occurrences (13) than the other two.

## 3.3 Physical properties

Besides transition temperatures, the other properties evaluated were density, thermal conductivity, and specific heat capacity.

The results of varying the density of the *am* and *sc* surrogates can be seen in Figure 4a and 4b, respectively. The values utilized were 800, 1,100, and 1,400 $kg \cdot m^{-3}$. No alteration in dripping starting time was registered for any variations in the respective groups. The dripping curves of the runs nearly overlapped, especially in the *sc* simulations. The density value applied to *am* (1,100 $kg \cdot m^{-3}$) had the lowest dripping occurrence for this group (10). In the *sc* group, the difference in dripping occurrence between the runs did not start until 25 s into the simulation and was very slight. Thus, the observed effect of varying the density was minor.

The results of varying thermal conductivity for *am* and *sc* simulations are shown in Figure 4c and d, respectively. The values utilized were 0.10, 0.27, and 0.45 $W \cdot m^{-1} \cdot K^{-1}$. Increasing the thermal conductivity of *am* materials increased the dripping occurrence: it went from 7, to 10, and then 14. The lowest *k* value (0.10 $W \cdot m^{-1} \cdot K^{-1}$) delayed the start of dripping (from 6/7 to 10 s). For *sc* materials, the start of dripping was at around 12 s for all runs. However, the lowest thermal conductivity (0.10 $W \cdot m^{-1} \cdot K^{-1}$) delayed the dripping considerably in comparison to the others, with the second occurrence 23 s into the simulation, for example. Consequently, the number of dripping occurrences was also lowest (6 as opposed to 13 in the other runs). The observed effect of varying the thermal conductivity was thus significant.

Results of varying the specific heat capacity for *am* and *sc* simulations are shown in Figure 4e and f, respectively. The values utilized were 1,000, 1,500, and 2,000 $J \cdot kg^{-1} \cdot K^{-1}$. A similar effect was noticed for both groups: the higher the Cp and the lower the dripping occurrence. For *am* materials, the dripping occurrences decreased from 17, to 10, and 8. Additionally, the lower value and the middle value of Cp (1,000 and 1,500 $J \cdot kg^{-1} \cdot K^{-1}$) started dripping at the same time (7 s), while the higher Cp value (2,000 $J \cdot kg^{-1} \cdot K^{-1}$) showed a significant delay (12 s). A larger effect was noticed for *sc* materials, where in addition to the lower dripping occurrence (from 18, to 13, and 9), increasing Cp also further delayed the start of dripping (from 5, to 13, and 18 s). The observed effect of varying the specific heat capacity was thus significant.

## 3.4 Material heat fluxes

Results on the variations of heat of decomposition ($H_{dec}$) and of the effective heat of combustion (EHC) are shown in Figure S1. These properties had somewhat surprisingly minor influence on dripping. It seems that the dripping as efficient cooling effect compensates somehow the increase in heat impact. Dripping is a complex response governed by an interplay of heating up, pyrolysis, viscosity, and so on; thus, no easy straightforward rules between dripping and heat impact must be expected. Nevertheless, the results also indicate the need of further investigations based on a refined model.

## 3.5 Char

To continue with the viscosity evaluation, new curves based on *am_c* and *sc_c* were designed to account for different char increments after $T_d$ (Figure 5a and b, respectively). The rate at which viscosity increases or decreases after $T_d$ has been related to the decomposition mechanism (13). In the model, this increase was simply related to the estimated speed of cross-linking. The faster the speed, the higher the amount of char formed. The $T_g$, $T_m$, and $T_d$ used were set at the same values as in Table 2 for all runs. Char contents of 0, 10, 30, and 50% were used.

For amorphous materials (Figure 5c), the increase in char content increased the delay in the start of dripping

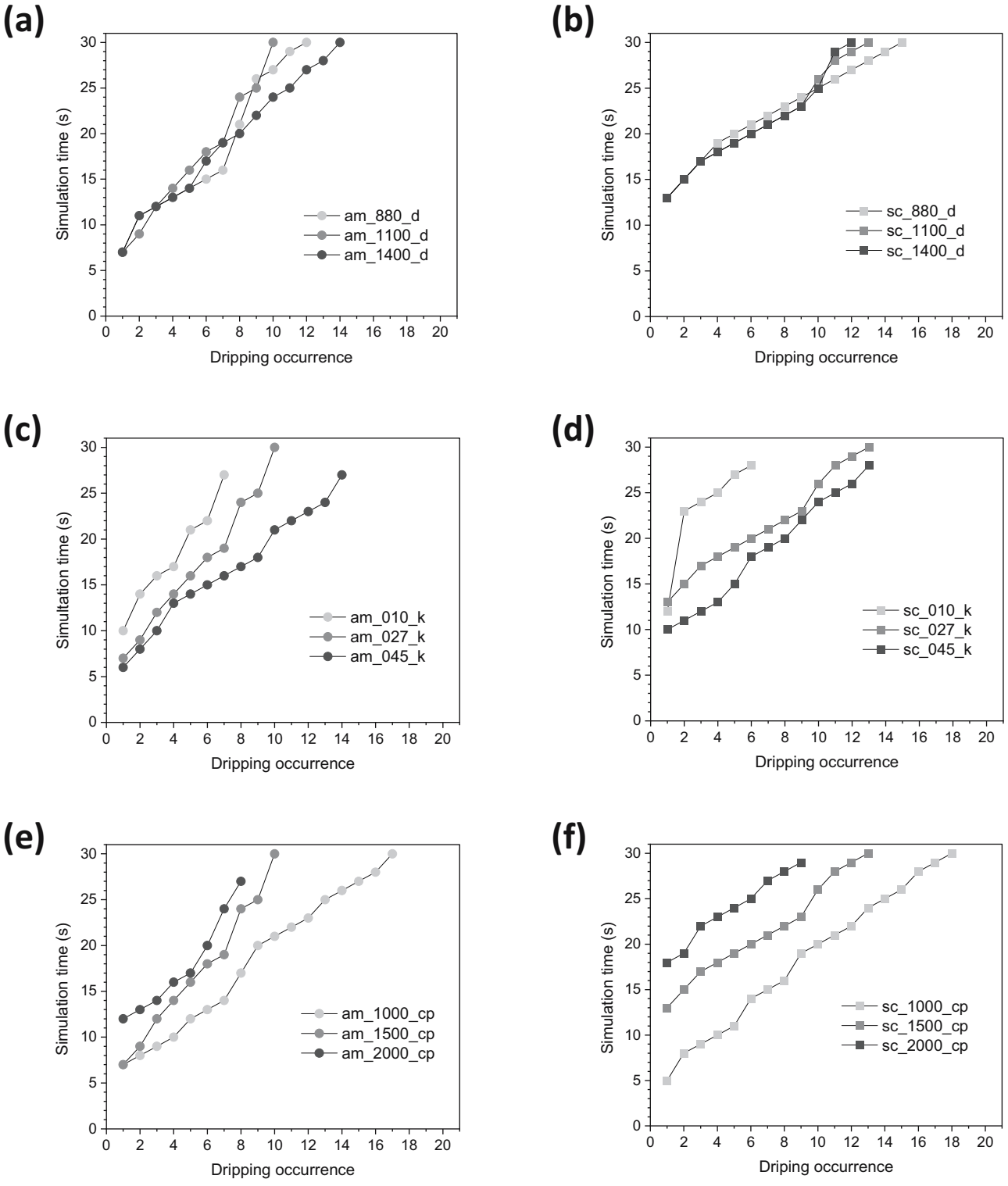


**Figure 4:** Results of varying the density (a) for am, (b) for sc, thermal conductivity (c) am, (d) sc, and specific heat (e) am, and (f) sc.

(from 7, to 10, 13, and 14 s). Although the resistance to dripping was enhanced, the dripping occurrence remained almost the same (10/11). On the other hand, dripping was strongly reduced for semi-crystalline materials when char content was increased (Figure 5d). Against the *sc* neat run, which had 13 dripping occurrences, the *sc_10%* run presented 7, while the *sc_30%* run presented only one dripping occurrence, and finally, *sc_50%* presented no dripping. The

start of dripping was also delayed with increased char content, but in a narrower range (from 13, to 14, and 16). Clearly, char yield had a relevant role in the decrease of dripping behaviour. Thus, the simulated results approximated those observed experimentally (see Section 3.6).

## 3.6 Validation of the viscosity method

The benchmark materials consisted of four thermoplastics, each with its own structural characteristics that determine their performance (see Figure S2). For instance, PMMA has pendant $CH_3$ groups which hinder the crystalline packing of the aliphatic polymer chains. Thus, it has the property of transparency and is defined as an amorphous thermoplastic. PA6 is classified as an engineering thermoplastic and has a wide range of applications. Its aliphatic structure and absence of large pendant groups permit a semi-crystalline arrangement of the chains. PEEK is a highly crystalline polymer formed by an aromatic main chain that promotes its noted chemical and mechanical properties allied with its high heat resistance. PSU is an amorphous and transparent material known for its toughness and stability at high temperatures, formed by an aromatic main chain.

Besides the configuration of the molecules (main chain and volume of the groups), the flow capacity is related to molecular weight ($M_w$) and decomposition aspects. The $M_w$ of these materials has been reported as 113.16 g·mol$^{-1}$ (PA6), 288.31 g·mol$^{-1}$ (PEEK), 100.12 g·mol$^{-1}$ (PMMA), and 442.53 g·mol$^{-1}$ (PSU). Thermogravimetry and rheology at low shear rates were measured and are displayed in Figure S3. PEEK and PSU had the highest heat resistances observed and produced the most residue (50.0 and 33.0 wt%, respectively), due to the

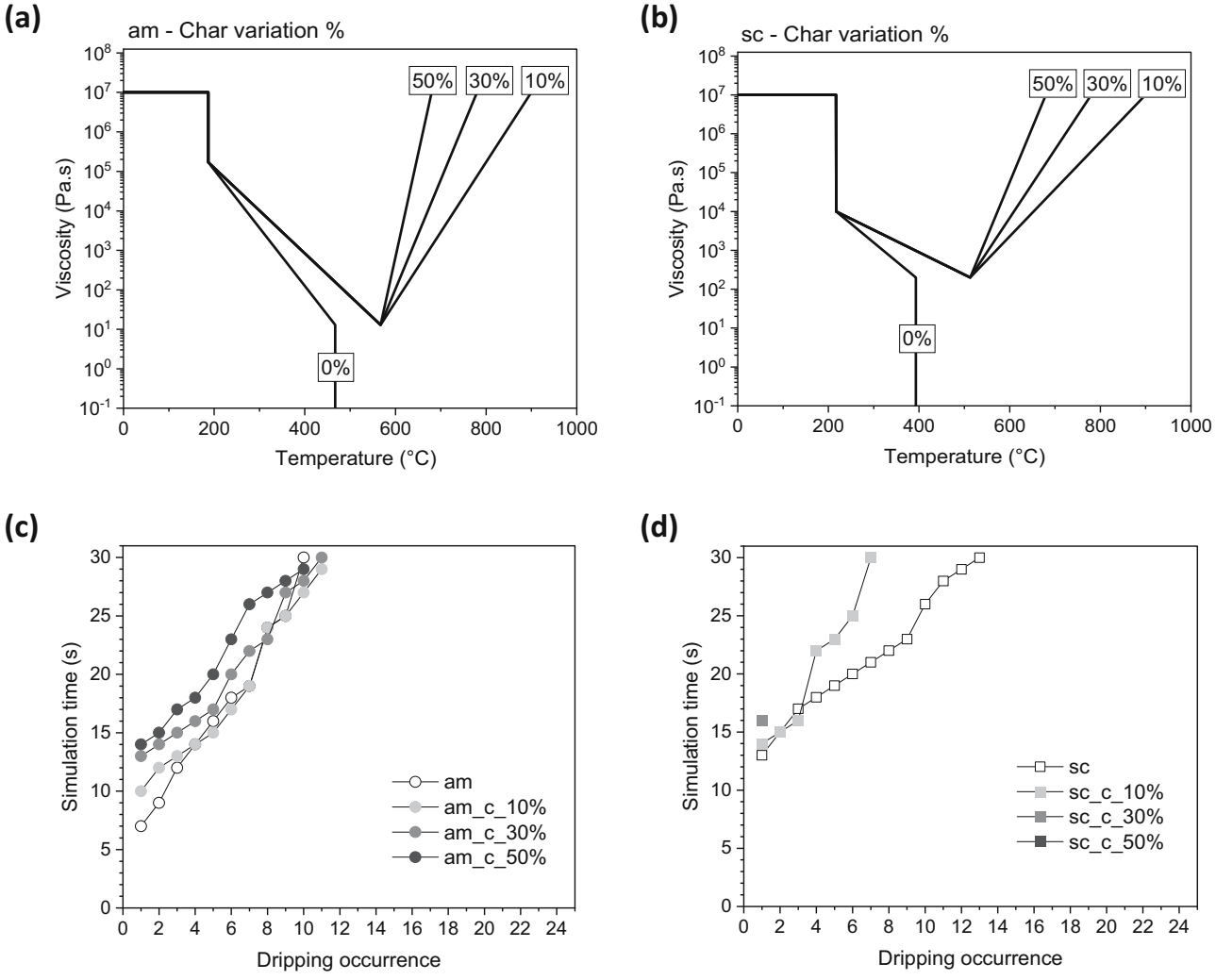


**Figure 5:** Curves designed for different char content materials (a and b) and the respective results (c and d).

**Table 3:** Characteristics of the benchmarks

| Characteristic | PA6 | PSU | PEEK | PMMA |
|---|---|---|---|---|
| UL-94 classification (3 mm) | V-2 | V-1 | V-0 | HB |
| Dripping | ✓ | ✗ | ✗ | ✓ |
| Dripping start time (s) | 12 | — | — | 26 |
| Density ($\rho$; kg·m$^{-3}$) | 1,110 | 1,208 | 1,234 | 1,366 |
| Glass transition temperature ($T_g$; °C) | 55 | 190 | 148 | 117 |
| Melting temperature ($T_m$; °C) | 216 | — | 343 | — |
| Decomposition temperature ($T_d$; °C) | 449 | 526 | 587 | 377 |
| Thermal conductivity ($k$; W·m$^{-1}$·K$^{-1}$) | 0.27 | 0.20 | 0.29 | 0.21 |
| Specific heat capacity (Cp; J·g$^{-1}$·K$^{-1}$) at 2°C | 1.64 | 1.09 | 1.51 | 1.32 |
| Activation energy ($E_a$; kJ·mol$^{-1}$) | 181.81 | 215.94 | 271.92 | 294.35 |
| Arrhenius coefficient ($A$; s$^{-1}$) | $1.4 \times 10^{11}$ | $1.3 \times 10^{12}$ | $3.2 \times 10^{14}$ | $4.4 \times 10^{21}$ |
| Char yield (CY; %) | 0.9 | 33.0 | 50.0 | 0.3 |
| Effective heat of combustion (EHC; J·g$^{-1}$) | 31.0 | 22.4 | 15.3 | 24.8 |
| Heat of decomposition ($H_{dec}$; J·g$^{-1}$) | 1,390 | 830 | 2,540 | 870 |

aromatic chains' tendency to cross-link at high temperatures. At the shear rate of 0.1 s$^{-1}$, the complex viscosity of the benchmarks increased as follows: PSU > PMMA > PEEK > PA6. Table 3 summarizes other properties of the benchmark materials from characterization and the literature. The decomposition temperature ($T_d$) was the peak temperature of the DTG curve (first differential thermogravimetry curve). Char yield was the residue remaining at 90°C in the thermogravimetric curves measured.

Each material achieved a different UL94 test classification. The V-0 and V-1 materials (PEEK and PSU) did not produce drops, while the V-2 and HB materials (PA6 and PMMA) produced dripping. PA6 presented melt deformation of the specimen, with a filament characteristic that led to small-sized flaming drops. Details on the behaviour of PA6 can be found in (21). The behaviour of PMMA during test is depicted in Figure S4. PMMA burns completely with only one flame application producing smoke and large flaming drops. This behaviour is due to the decomposition mechanism of PMMA, which is depolymerization by end-chain scission. After flame removal, dripping started very late, but once it started the dripping occurred steadily with about one drop falling each following second. The tested extremities of the non-dripping specimens (PSU and PEEK) are shown in Figure S4 too. The area affected by fire was larger for PSU than for PEEK, as can be noticed by the char left behind in the specimens after test. PSU, as a sulphonated polymer, has a self-flame-retardancy characteristic and does not ignite. PEEK burned at the edges of the specimen tip only when the flame was applied.

In another simple experiment, the non-dripping materials were subjected to a small flame for an extended period of time (2 min). The response of PEEK remained non-dripping, meaning that in this material structure, dripping has no space to compete with gasification and mostly charring. PSU, in contrast, ignited in some tests and produced flaming drops after the flame removal, meaning that under different conditions dripping can compete with charring and mostly gasification.

Analysing the data from Table 3 shows that the properties roughly correspond with the surrogates: PA6 as *sc*, PEEK as *sc_c*, PMMA as *am*, and PSU as *am_c*. However,

**Table 4:** Dripping responses

| Material | Correspondent | Experimental* | Simulated | |
|---|---|---|---|---|
| | | | Measured viscosity* | Surrogates' viscosity |
| PA6 | *sc* | Dripping (12 s; 2) | Dripping (12 s; 5) | — |
| PEEK | *sc_c* | Non-dripping | Dripping (21 s; 6) | Non-dripping |
| PMMA | *am* | Dripping (26 s; 1) | Dripping (22 s; 4) | — |
| PSU | *am_c* | Non-dripping | Dripping (14 s; 10) | Non-dripping |

*The () contains: the dripping start time (in seconds); the number of dripping occurrences in 30 s. For experimental column, it refers to dripping occurrences originated from the 10 s of flame application plus 20 s of after-flame time, to agree to the simulation time.

when the specific data for each of these materials were used to simulate their respective behaviour in the PFEM model, the dripping response was not satisfactory for PEEK and PSU (Table 4). This was because their viscosities were not measured above $T_d$. Once the surrogates' viscosities were used along with the specific properties of these benchmarks, the results agreed with the experimental ones.

# 4 Conclusion

Aiming for a better understanding of the dripping behaviour of thermoplastics, a parametric analysis was performed in a modelled UL94 vertical test scenario by PFEM. Due to the limits/boundaries used in the simulations (surrogates), the key parameters for dripping behaviour were identified as exerting larger or minor effects. Density had the least influence on dripping assessed in this work. Higher thermal conductivity generated more dripping, and allowed it to start earlier. The specific heat capacity, which represents the heat transfer potential of the material, had the greatest impact on dripping occurrence and start (decreasing both by enhancing Cp). A minor influence by the heat of decomposition and heat of combustion of the volatiles was observed. Char content improved dripping resistance, especially for materials defined as *sc*. Given the complexity of dripping behaviour and the limitations of the PFEM model applied the agreement between experimental and simulated results was considered good. The difficulty in obtaining viscosity values at high temperatures as input was solved by using the standard curves defined for the surrogates.

**Acknowledgements:** The authors thank the National Council of Technological and Scientific Development of Brazil (CNPq) for its financial support (205385/2014-1). The authors thank Dr. Julio Marti for his support on the PFEM set-up, and also CIMNE, especially for the GiD licence kindly provided for our work. A.T.S.D. thanks the TU Berlin for the support with a STIBET degree completion grant.

**Conflict of interest:** Authors state no conflict of interest.

# References

(1) Ohlemiller TJ, Butler K. Influence of polymer melt behaviour on flammability. Gaithersburg MD: NIST Rep no NISTIR 6588; 2000.
(2) UL 94 Standard. IEC 60695-11-10. 50W (20mm) Vertical Burning Test.
(3) Joseph P, Tretsiakova-McNally S. Melt-flow behaviours of thermoplastic materials under fire conditions: recent experimental studies and some theoretical approaches. Materials. 2015;8:8793–8803. doi: 10.3390/ma8125492.
(4) Kempel F, Schartel B, Marti JM, Butler KM, Rossi R, Idelsohn SR, et al. Modelling the vertical UL 94 test: competition and collaboration between melt dripping, gasification, and combustion. Fire Mater. 2015;39:570–84. doi: 10.1002/fam.2257.
(5) Zhao HB, Liu BW, Wang XL, Chen L, Wang XL, Wang YZ. A flame-retardant-free and thermo-cross-linkable copolyester: Flame-retardant and anti-dripping mode of action. Polymer. 2014;55:2394–403. doi: 10.1016/j.polymer.2014.03.044.
(6) Guo DM, Fu T, Ruan C, Wang XL, Chen L, Wang YZ. A new approach to improving flame retardancy, smoke suppression and anti-dripping of PET: Via arylene-ether units rearrangement reactions at high temperature. Polymer. 2015;77:21–31. doi: 10.1016/j.polymer.2015.09.016.
(7) Wu JN, Qin ZH, Chen, Liu BW, Wang XL, Wang YZ. Tailoring Schiff base cross-linking by cyano group toward excellent flame retardancy, anti-dripping and smoke suppression of PET. Polymer. 2018;153:78–85. doi: 10.1016/j.polymer.2018.08.004.
(8) Dittrich B, Wartig KA, Hofmann D, Mülhaupt R, Schartel B. Flame retardancy through carbon nanomaterials: Carbon black, multiwall nanotubes, expanded graphite, multi-layer graphene and graphene in polypropylene. Polym Degrad Stab. 2013;98:1495–505. doi: 10.1016/j.polymdegradstab.2013.04.009.
(9) Zhang Y, Ni YP, He MX, Wang XL, Chen L, Wang YZ. Phosphorus-containing copolyesters: The effect of ionic group and its analogous phosphorus heterocycles on their flame-retardant and anti-dripping performances. Polymer. 2015;60:50–61. doi: 10.1016/j.polymer.2015.01.030.
(10) Liu BW, Lei YF, Liu XF, Guo DM, Chen L, Wang YZ. Thermally induced end-group-capturing as an eco-friendly and general method for enhancing the fire safety of semi-aromatic polyesters. Polymer. 2021;218:123430. doi: 10.1016/j.polymer.2021.123430.
(11) Pawlowski KH, Schartel B. Flame retardancy mechanisms of triphenyl phosphate, resorcinol bis(diphenyl phosphate) and bisphenol A bis(diphenyl phosphate) in polycarbonate/acrylonitrile–butadiene–styrene blends. Polym Int. 2007;56:1404–14. doi: 10.1002/pi.2290.
(12) Wang Y, Zhang F, Chen X, Jin Y, Zhang J. Burning and dripping behaviors of polymers under the UL 94 vertical burning conditions. Fire Mater. 2010;34:203215. doi: 10.1002/fam.1021.
(13) Wang Y, Jow J, Su K, Zhang K. Dripping behavior of burning polymers under UL 94 vertical test conditions. J Fire Sci. 2012;30:477–501. doi: 10.1177/073490411244612.
(14) Kandola BK, Price D, Milnes GJ, Da Silva A, Gao F, Nigmatullin R. Characterization of Melt dripping behavior of flame retarded polypropylene nanocomposites. Chapter 21 in Fire and Polymers VI: New Advances in Flame Retardant Chemistry and Science. Vol. 1118; 2012. p. 311–25. ACS Symposium. Series doi: 10.1021/bk-2012-1118.ch021.
(15) Wang Y, Zhang J. Thermal stabilities of drops of burning thermoplastics under the UL 94 vertical test conditions. J Hazard Mater. 2013;246–247:103–9. doi: 10.1016/j.jhazmat.2012.12.020.
(16) Kandola BK, Price D, Milnes GJ, Da Silva A. Development of a novel experimental technique for quantitative study of melt dripping of thermoplastic polymers. Polym Degrad Stab. 2013;98:52–63. doi: 10.1016/j.polymdegradstab.2012.10.028.
(17) Kandola BK, Ndiaye N, Price D. Quantification of polymer degradation during melt dripping of thermoplastic polymers. Polym Degrad Stab. 2014;106:16–25. doi: 10.1016/j.polymdegradstab.2013.12.020.
(18) Dupretz R, Fontaine G, Duquesne S, Bourbigot S. Instrumentation of UL-94 test: understanding of mechanisms involved in fire

retardancy of polymers. Polym Adv Technol. 2015;26:865–73. doi: 10.1002/pat.3507.
(19) Hu C, Fontaine G, Tranchard P, Delaunay T, Collinet M, Marcille S, et al. In-situ investigation of temperature evolution of drippings via an optimized UL-94 instrumentation: application to flame retarded polybutylene succinate. Polym Degrad Stab. 2018;155:145–52. doi: 10.1016/j.polymdegradstab.2018.07.015.
(20) Matzen M, Kandola BK, Huth C, Schartel B. Influence of flame retardants on the melt dripping behaviour of thermoplastic polymers. Materials. 2015;8:5621–46. doi: 10.3390/ma8095267.
(21) Turski Silva Diniz A, Huth C, Schartel B. Dripping and decomposition under fire: Melamine cyanurate vs glass fibres in polyamide 6. Polym Degrad Stab. 2020;171:109048. doi: 10.1016/j.polymdegradstab.2019.109048.
(22) Turski Silva Diniz A, Marti JM, Schartel B. High heat resistance can be deceiving: dripping behavior of polyamide 4.6 in fire. Macromol Mater Eng. 2023;308:2300091. doi: 10.1002/mame.202300091.
(23) Yueming Y, Liangdong X, Miaohong Y, Linghui L, Zhang Y, Huo S, et al. Governing effects of melt viscosity on fire performances of polylactide and its fire-retardant systems. iScience. 2022;25:103950. doi: 10.1016/j.isci.2022.103950.
(24) Seah DGJ, Dasari A. Understanding the influence of melt dripping on UL94 test response in a PA11 system. Polym Test. 2023;118:107893. doi: 10.1016/j.polymertesting.2022.107893.
(25) Wang Y, Kang W, Zhang X, Chen C, Sun P, Zhang F, et al. Development of a pendant experiment using melt indexer for correlation with the large-size dripping in the UL-94 test. Fire Mater. 2018;42:436–46. doi: 10.1002/fam.2510.
(26) Spieß B, Metzsch-Zilligen E, Pfaendner R. Mechanistic evaluation of flame retardants during UL94 standard testing via IR-camera. Polym Test. 2021;103:107320. doi: 10.1016/j.polymertesting.2021.107320.
(27) Matzen M, Marti J, Oñate E, Schartel B. Particle finite element modelling and advanced experiments on dripping-V-0-classified polypropylene. Proceedings of the 15th International Conference and Exhibition – Fire and Materials. San Francisco, CA, USA; 2017, 6–8 February 2017.
(28) Spieß B, Metzsch-Zilligen E, Pfaendner R. A new class of oxyimides: Oxyimide ethers and their use as flame retardants. Macromol Mater Eng. 2021;306:2000650. doi: 10.1002/mame.202000650.
(29) Wu H, Ortiz R, De Azevedo Correa R, Krifa M, Koo JH. Self-extinguishing and non-drip flame retardant polyamide 6 nanocomposite: Mechanical, thermal, and combustion behavior. Flame Retardancy Therm Stab Mater. 2018;1(1):1–13. doi: 10.1515/flret-2018-0001.
(30) Yu W, Yang W, Xu P, Dai C, Liu Q, Ma P. Simultaneously enhance the fire safety and mechanical properties of PLA by incorporating a cyclophosphazene-based flame retardant. e-Polymers. 2022;22(1):411–29. doi: 10.1515/epoly-2022-0041.
(31) Battig A, Abdou-Rahaman Fadul N, Frasca D, Schulze D, Schartel B. Multifunctional graphene nanofiller in flame retarded polybutadiene/chloroprene/carbon black composites. e-Polymers. 2021;21(1):244–62. doi: 10.1515/epoly-2021-0026.
(32) Oñate E, Idelsohn S, Del Pin F, Aubry R. The particle finite element method. An overview. Int J Numer Meth Engin. 2004;1:267–307. doi: 10.1142/S0219876204000204.
(33) Oñate E, Rossi SR, Idelsohn R, Butler KM. Melting and spread of polymers in fire with the particle finite element method. Int J Numer Meth Eng. 2010;81:1046–72. doi: 10.1002/nme.2731.
(34) Marti J, Schartel B, Oñate E. Simulation of the burning and dripping cables in fire using the particle finite element method. J Fire Sci. 2022;40:3–25. doi: 10.1177/07349041211039752.
(35) Marti J, Idelsohn SR, Oñate E. A finite element model for the simulation of the UL-94 burning test. Fire Technol. 2018;54:1783–805. doi: 10.1007/s10694-018-0769-0.
(36) Marti J, De la Vega J, Wang DY, Oñate E. Numerical simulation of flame retardant polymers using a combined eulerian-lagrangian finite element formulation. Appl Sci. 2021;11:5952. doi: 10.3390/app11135952.
(37) Kempel F, Schartel B, Linteris GT, Stoliarov SI, Lyon RE, Walters RN, et al. Prediction of the mass loss rate of polymer materials: Impact of residue formation. Combust Flame. 2012;159:2974–84. doi: 10.1016/j.combustflame.2012.03.012.
(38) Stoliarov SI, Safronava N, Lyon RE. The effect of variation in polymer properties on the rate of burning. Fire Mater. 2009;33:257–71. doi: 10.1002/fam.1003.
(39) Linteris GT. Numerical simulations of polymer pyrolysis rate: Effect of property variations. Fire Mater. 2011;35:463–80. doi: 10.1002/fam.1066.
(40) McCoy CG, Stoliarov SI. Experimental characterization and modeling of boundary conditions and flame spread dynamics observed in the UL-94V test. Combust Flame. 2021;225:214–27. doi: 10.1016/j.combustflame.2020.10.05.
(41) McCoy CG, Stoliarov SI. Prediction of UL-94V tests performed on a wide range of polymeric materials using a comprehensive pyrolysis model coupled with an empirical flame heat feedback model. Fire Mater. 2022;46:905–18. doi: 10.1002/fam.3038.
(42) Cremonesi A, Franci A, Idelsohn S, Oñate E. A state of the art review of the particle finite element method (PFEM). Arch Comput Methods Eng. 2020;27:1709–35. doi: 10.1007/s11831-020-09468-4.
(43) Hamins A, Bundy M, Dillon SE. Characterization of candle flames. J Fire Prot Eng. 2005;15:265–85. doi: 10.1177/1042391505053163.
(44) Stoliarov SI, Walters RN. Determination of the heats of gasification of polymers using differential scanning calorimetry. Polym Degrad Stabil. 2008;93:422–7. doi: 10.1016/j.polymdegradstab.2007.11.022.
(45) Bourbigot S. Evaluation of condensed phase: char/residue analysis. In: Vahabi H, Saeb MR, Malucelli G, editors. Chapter 6 in Analysis of Flame Retardancy in Polymer Science. Elsevier; 2022 doi: 10.1016/B978-0-12-824045-8.09991-3.
(46) Lyon RE. Plastics and rubber Chapter 3 in Handbook of building materials for fire protection. In: Harper CA, editor. New York: McGraw-Hill; 2004.
(47) Kim Y, Hossain A, Nakamura Y. Numerical modeling of melting and dripping process of polymeric material subjected to moving heat flux: Prediction of drop time. Proc Combust Inst; 2015;35:2555–62. doi: 10.1016/j.proci.2014.05.068.